Soft Matter

PAPER

A microscopic view of graphene-oxide/poly(acrylic acid) physical hydrogels: effects of polymer charge and graphene oxide loading†

Kostas Karatasos ID *[ab] and Georgios Kritikos[a]

In this work we have examined in detail by means of fully atomistic molecular dynamics simulations, physical hydrogels formed by a polymer electrolyte, poly(acrylic acid), and graphene oxide, at two different charging states of the polymer and two different graphene oxide concentrations. It was found that variations of these parameters incurred drastic changes in general morphological characteristics of the composite materials, the degree of physical adsorption of polyelectrolyte chains onto the graphene oxide surface, the polymer dynamic response at local and global length scales, in the charge distributions around the components, and in the mobility of the counterions. All these microscopic features are expected to significantly affect macroscopic physical properties of the hydrogels, such as their mechanical responses and their electrical behaviors.

1. Introduction

Hydrogels are soft materials characterized by a 3-dimensional structure with high water content. They have attracted intense scientific and technological interest due to their potential use in areas such as in biomedicine,[1–5] environmental studies,[6,7] sensors,[8,9] and soft matter engineering,[10] *etc.* They can be generally categorized as physically and chemically crosslinked. Physically crosslinked hydrogels are easier to form, are devoid of biomedically hazardous crosslinking agents, and exhibit structural reversibility,[11] but they are generally weak, thus limiting the area of their applicability.[12] Both categories of hydrogels may also suffer from limited porosity, usually lower than desired absorption capacity, slow response times, and structural instability under the application of external stimuli.[13]

To remedy such problems and to improve overall hydrogels performance, hybrid systems usually involving polymeric compounds reinforced with nano-additives have been widely studied.[14–17] Among the different nano-inclusions which have been used to enhance the properties of hydrogels, graphene oxide (GO) has recently been considered as a promising candidate. GO bearing oxygen groups such as hydroxyls, carboxyls and epoxides, is soluble in water and interacts favorably with a wide range of polymer matrices, thus allowing a good dispersion and therefore the fabrication of structurally and thermally stable hydrogels.[3,18–25]

A specific category of GO-based hydrogels is one that involves polymer electrolytes. These hydrogels are of particular importance due to their responsiveness to changes in local environment, such as pH.[26] In such pH-sensitive systems, the ability to regulate the degree of ion dissociation renders them appropriate candidates for controlled drug release purposes,[23,27] while their selectivity in the adsorption or exclusion of ionic moieties depending on their charge makes them interesting for membrane technology for water filtering[28] *via* processes such as forward or reverse osmosis.[29–31]

Control of key macroscopic properties of such hydrogels is based on molecular-level details associated with the relative percentage of the components in the mixture,[18] the characteristics of the dispersion of the constituents in the aqueous phase,[20] the nature of the interactions between the filler and the polymer,[24,32] the dynamic behavior of the components,[33] and in the case of electrically active systems, the electrostatic environment as this is described by the charge distribution around the components, the dielectric permittivity of the solvent, and the presence or absence of salt ions.[34,35]

The aim of the present study is to contribute toward a molecular-level description of the aforementioned parameters in such systems utilizing computer simulations, by examining in detail aqueous dispersions of GO and a polymer electrolyte, poly(acrylic acid) (PAA). Recent experimental studies have demonstrated the increasing scientific and technological interest in GO/PAA hydrogels, by exploring the ability of GO to act as a

[a] Laboratory of Physical Chemistry, Department of Chemical Engineering, Aristotle University of Thessaloniki, 54124 Thessaloniki, Greece. E-mail: karatas@eng.auth.gr; Fax: +30-2310-996222; Tel: +30-2310-995850
[b] Institute of Electronic Structure and Laser, Foundation for Research and Technology – Hellas, P. O. Box 1527, 711 10 Heraklion Crete, Greece

physical crosslinker in order to form mechanically enhanced GO/PAA composites[36] for their swelling, mechanical, and electro responsive properties,[37,38] their thermal and pH responsiveness,[26] their ability to self-heal,[39] their capacity to be used as replacements for metal-foil current collectors in lithium-ion batteries,[40] and as highly efficient adsorbents.[31]

The hydrogels examined in this work were comprised by PAA chains and GO nanosheets at two different GO loadings and at two different charging states of the polymer (corresponding to different pH conditions), together with water molecules (at a high content) and neutralizing sodium counterions. These models essentially represent physical hydrogels where only non-covalent interactions are present between the different molecular components. To get a more detailed picture, we opted to utilize molecular dynamics (MD) simulations in the explicit atomic representation so that all necessary information regarding the pertinent mechanisms which operate at the atomic level becomes accessible.

To our knowledge, this is the first fully atomistic simulation study of PAA/GO aqueous dispersions.

2. Systems description and simulation details

In total, 6 models were simulated: 4 GO/PAA/water/counterion systems and 2 PAA/water/counterion systems that were used as references. Their characteristics are described in Table 1. In all models 30 PAA chains were included in their atactic form, comprised by 40 monomers each. In their fully charged state each monomer was negatively charged ($-1e$, where e represents the charge of an electron, arising from the ionized COO^- group), while in their semi-charged state every other monomer of a chain was negatively charged ($-1e$). For the PAA/water systems the two charging states examined, $i.e.$, 50% and 100%, correspond to conditions of pH $\cong$ 6.5 and $\geq$10 respectively; however, in the presence of GO this correspondence might not be exact.[41] Therefore, in order to avoid any misconception, we will henceforth refer to the degree of PAA charging rather than to the pH value of the systems. In the graphene-oxide-containing models the GO loading was kept between 2 wt% and 4 wt% and the water content at 90 wt% and higher, which are close to experimentally studied similar hydrogels.[37,42]

Each graphene-oxide flake was modelled with a carbon to oxygen atom ratio close to 5 : 1 and a hydroxyl to epoxy group ratio of 3 : 2 approximately, following previous works[43,44] and terminated with hydrogen atoms as depicted in Fig. 1.
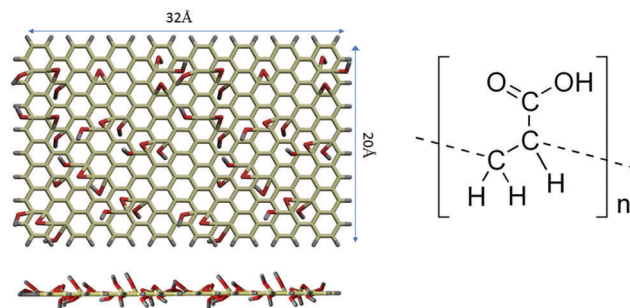

Fig. 1 Schematic of a GO sheet in frontal and side view (left) and of a PAA monomer (right). In the GO model, oxygens are shown in red, hydrogens in grey and carbons in dark yellow.

Partial charges for the carbon and oxygen atoms of GO were assigned according to ref. 43 together with the atomic interaction parameters which were based on the AMBER forcefield.[45] For compatibility issues and following recent studies on PAA,[46,47] the energetic parameters describing the polymer atoms were also taken from the AMBER forcefield.[45,48] Partial charges for PAA atoms were assigned using the Gasteiger method as implemented in the AMBER Antechamber module.[49] Water molecules were modelled according to the TIP3P model.[50] The dimensions of the GO flakes were kept at the nanoscale in order to be comparable to the average size of the polymer chains (their radius of gyration was estimated to be between 13 Å and 15 Å depending on the charging state of the chain, as will be discussed in Section 3.1). Such nanosized dispersions based on graphene and graphene oxide have recently been fabricated and studied experimentally.[51–53]

Starting configurations of all the models were prepared using the Packmol program.[54] All systems were simulated following the isothermal–isobaric (NPT) ensemble at temperature T = 300 K and pressure P = 1 bar. Prior to production runs, the systems were energy minimized and left to equilibrate via NPT MD for about 100 ns. Equilibration criteria involved stabilization of total and partial energies, density, average size of the polymer chains, and spatial arrangement of the molecular species in each model. The MD runs were performed under periodic boundary conditions with a timestep of 1 fs (using the r-RESPA algorithm for evaluation of the long-range interactions every two timesteps) and a frame-saving frequency of 10 ps (higher frame-saving frequencies were also used for short-length trajectories when needed for analysis purposes). Temperature control was performed utilizing the Langevin method (with a damping coefficient of 5 ps^{-1}) and pressure control by means of the Nose–Hoover Langevin piston method[55] (using a piston period of 0.1 ps and a decay time

Table 1 Details of the systems simulated

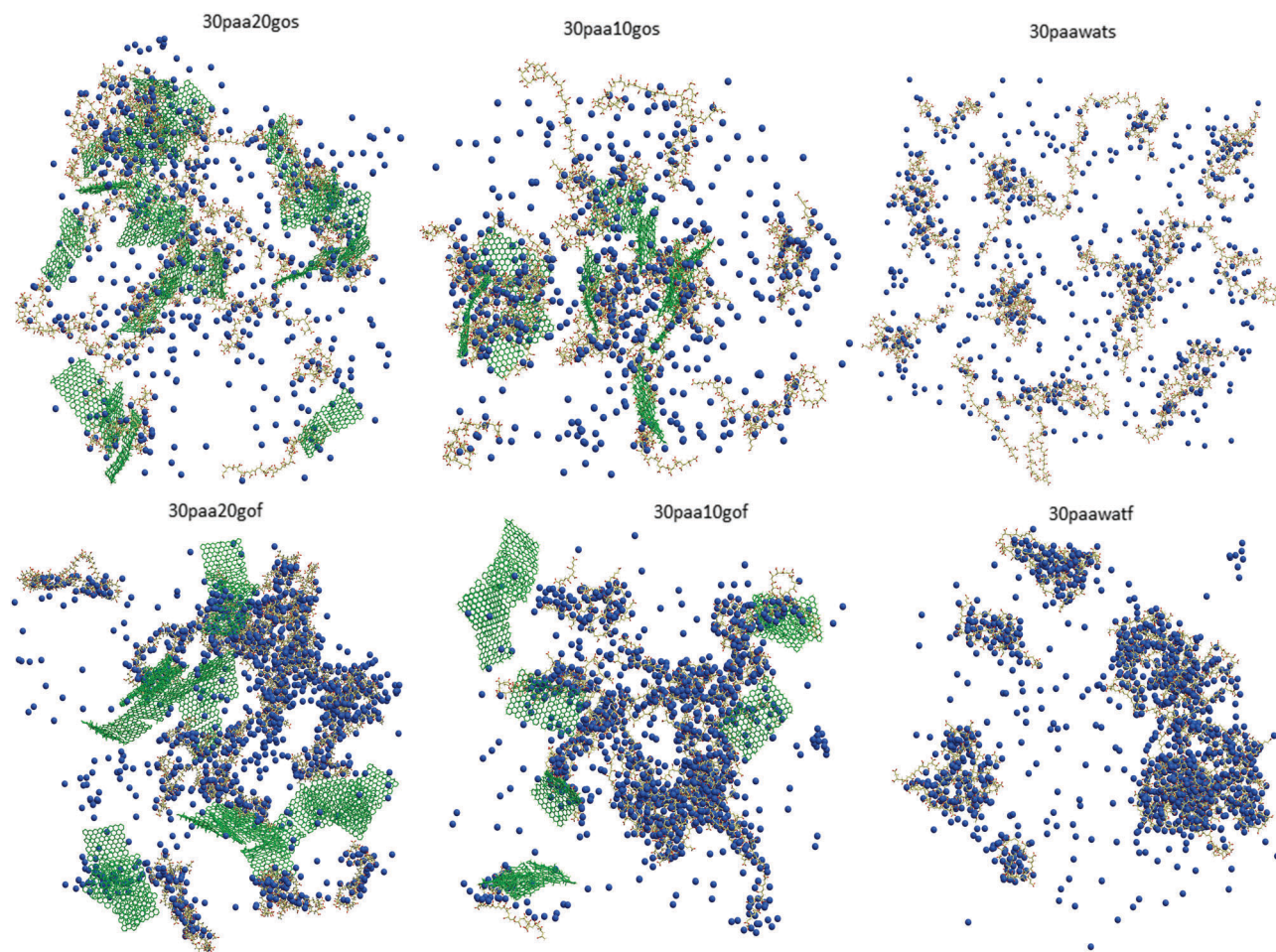| System notation	Total number of atoms	Number of PAA chains	Number of GO flakes	Degree of PAA charging %	Number of sodium counterions	GO wt%/ water wt%
30paa10gos	305 183	30	10	50	600	2.2/92.5
30paa10gof	330 503	30	10	100	1200	2.0/92.4
30paa20gos	334 543	30	20	50	600	4.0/91.2
30paa20gof	334 543	30	20	100	1200	4.0/90.6
30paawats	301 143	30	0	50	600	0/100
30paawatf	326 463	30	0	100	1200	0/100

Fig. 2   Snapshots of the simulated systems after equilibration. Water molecules are removed for clarity. GO flakes are shown in green, PAA chains in dark yellow and counterions as blue spheres.

of 0.05 ps). Electrostatic interactions were computed *via* the particle mesh Ewald (PME) scheme.[56] All simulations were performed with NAMD 2.12[57] with a distance cutoff of 12 Å for non-bonded interactions. Analysis was conducted by home-made routines.

Fig. 2 portrays snapshots of the examined models after equilibration (see Fig. S1 in ESI† for the as-constructed structures). Already from the snapshots one can distinguish differences in the arrangement of the polymer chains between the semi-charged and the fully charged systems, which will be discussed in more detail in the sections to follow. Regarding the GO dispersion characteristics, it appears that GO flakes tend to organize in oligomeric clusters, in line with previous works examining GO aqueous solutions,[58] as well as with the behavior of non-oxidized graphene flakes in the absence of solvent, where clusters formed by 2–3 platelets were noted.[59,60]

3. Results and discussion

3.1.   Chain conformational characteristics

Since the inner structure of a polymer composite hydrogel is intimately related to the chain conformations, through the way they affect the internal percolation pattern and ultimately its final properties,[18,31] it is of interest to check how PAA chains

respond to a change in their charging state in the presence of counterions and GO. To this end, we examined the distribution of the end-to-end distance of the PAA chains and grouped them according to the polymer's charging state, as depicted in Fig. 3.

In models with semi-charged chains the distributions appear to be broader and to extend to higher distances (notice the tail in these distributions towards longer distances), implying the presence of a subset of chains with more extended configurations. The distributions describing the models with the lower GO content show resemblance to those without GO, while those corresponding to the higher GO loading differentiate from the latter with respect to the location of the peaks (*i.e.*, the populations representing the most probable configurations). These observed differences can be quantified in terms of an experimentally accessible quantity, that of the average radius of gyrations, R_g, of the PAA molecules. Furthermore, we can obtain information regarding the shape asymmetry of the polymer chains through determination of the principal moments ($I_z > I_y > I_x$) which can be derived through diagonalization of the moment of inertia tensor

$$I = \sum_{i=1}^{N} m_i \left[(\mathbf{r}_i \times \mathbf{r}_i) \mathbf{l}_3 - \left(\mathbf{r}_i \mathbf{r}_i^T \right) \right] \qquad (1)$$
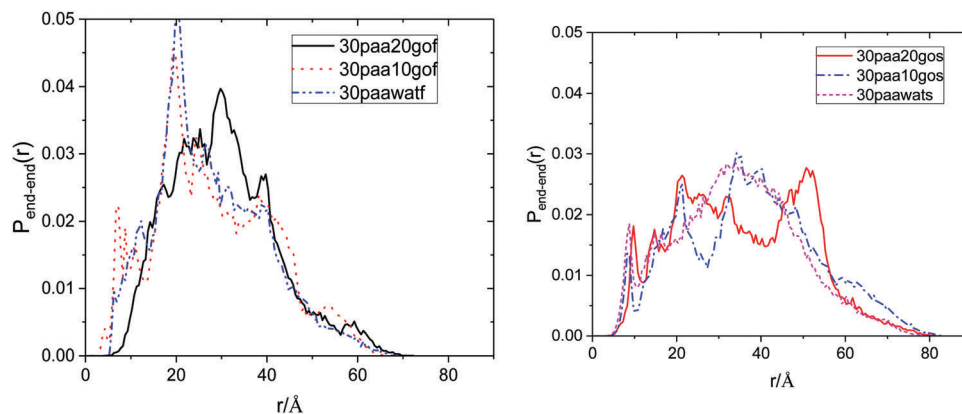
Fig. 3 Distributions of the end-to-end distance of PAA chains in models involving fully charged (left) and semi-charged (right) chains.

where $\mathbf{r}_i$ is the position vector of the ith atom relative to the center of mass of the molecule, N is the number of atoms per molecule, $\mathbf{l}_3$ is the unitary matrix of the 3rd order and m_i represents the mass of the ith atom. The eigenvalues of the inertia tensor denote the principal moments while the corresponding eigenvectors define the directions of the principal axes for each molecule. The degree of anisotropy in shape of the PAA chains can be estimated by calculating the asphericity parameter δ which is defined as[61]

$$\delta = 1 - 3\frac{\langle I_2 \rangle}{\langle I_1^2 \rangle} \qquad (2)$$

where $I_1 = I_x + I_y + I_z$ and $I_2 = I_xI_y + I_xI_z + I_yI_z$. The asphericity parameter ranges between the values of 0 and 1 which correspond to a spherical and to a rod-like shape, respectively. The average dimensions of the polymer chains as represented by their radius of gyration and parameter δ are listed in Table 2.

Focusing on the asphericity parameter, it appears that chains in the semi-charged models become more asymmetric in shape, while the presence of GO does not seem to impart significant changes. The higher shape anisotropy of the semi-charged PAA chains can be directly correlated with the larger radii of gyration, although the observed differences are not dramatic. This could be related[62] to the rather low molecular weights of the PAA chains examined here ($\sim$2884 g mol^{-1}). It is, however, noticeable that the semi-charged chains exhibit larger dimensions than their fully charged counterparts, despite carrying half as many like-charged monomers. To account for this observation, we have to consider the details of Coulombic screening provided by the sodium counterions.

3.2. Counterion condensation

To get an estimation of the counterion-induced degree of Coulombic screening experienced by the PAA chains, we calculated the pair distribution functions between Na$^+$ atoms and the charged oxygens belonging to the PAA COO$^-$ groups. This is shown in Fig. 4a. The sharp peak at a separation of $\sim$2.5 Å is indicative of counterion condensation upon the polymer chains. This behavior is in accord with the Manning criterion[63] for monovalent charged groups and counterions, $l_B/b \geq 1$ where l_B denotes the Bjerrum length of water and b the charged-group spacing along the PAA chain. Taking $l_B \cong 7$ Å for water at room temperature,[63] which is close to 300 K, considered here and separations between the charged oxygens of the COO$^-$ groups of $\sim$3 Å and $\sim$4.3 Å for fully charged and semi-charged PAA chains respectively, as found for our models, in all cases the Manning criterion for counterion condensation is satisfied.

By taking into account all pairs with separations less or equal to the location of the first minima in the pair distribution function of Fig. 4a, we were able to estimate the percentage of the condensed counterions, as illustrated in Fig. 4b. Evidently, the degree of counterion condensation on the fully charged chains ($\sim$75%) is considerably higher when compared to that characterizing their semi-charged analogues ($\sim$45%), thus providing a more effective electrostatic screening. The higher degree of electrostatic screening in the fully charged chains can account for the reduction in their average size (see Table 2), in line with experiments performed in polyelectrolyte solutions in the presence of salt ions.[64] Moreover, counterions condensed on the fully charged polymers appear to be much more localized as can be inferred both from Fig. 4a (higher/sharper peaks) and from the more intense peaks characterizing the corresponding charge distributions around a PAA chain (see Fig. S2 in the ESI†). On the other hand, the GO loading (at least within the examined range) does not seem to affect appreciably the percentage of the counterions condensed on PAA chains.

Given the importance of polymer/filler interactions in the electrical response of such GO/PAA hydrogels[40] it would also be informative to examine in more detail charge distributions close to the PAA/GO interface. Fig. 5 illustrates charge distributions of the sodium counterions and the PAA chains in a

Table 2 Average size and asphericity parameter of the PAA chains

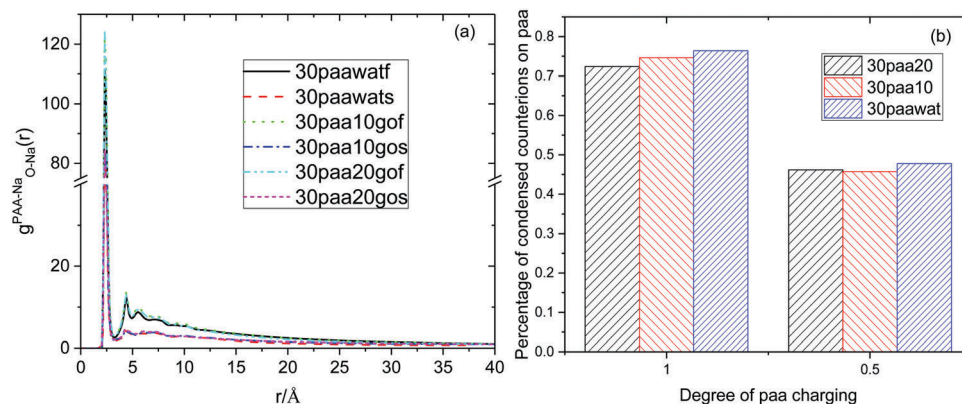| System	Radius of gyration/Å	δ
30paawats	14.89 ± 0.28	0.131 ± 0.007
30paa10gos	15.75 ± 0.63	0.130 ± 0.006
30paa20gos	15.52 ± 0.34	0.131 ± 0.005
30paawatf	12.79 ± 0.12	0.098 ± 0.003
30paa10gof	13.26 ± 0.21	0.108 ± 0.006
30paa20gof	13.87 ± 0.27	0.112 ± 0.005

Fig. 4 (a) Pair distribution functions between charged oxygens in the PAA COO⁻ groups and the Na⁺ counterions. (b) Degree of counterion condensation on the PAA chains in the examined models.
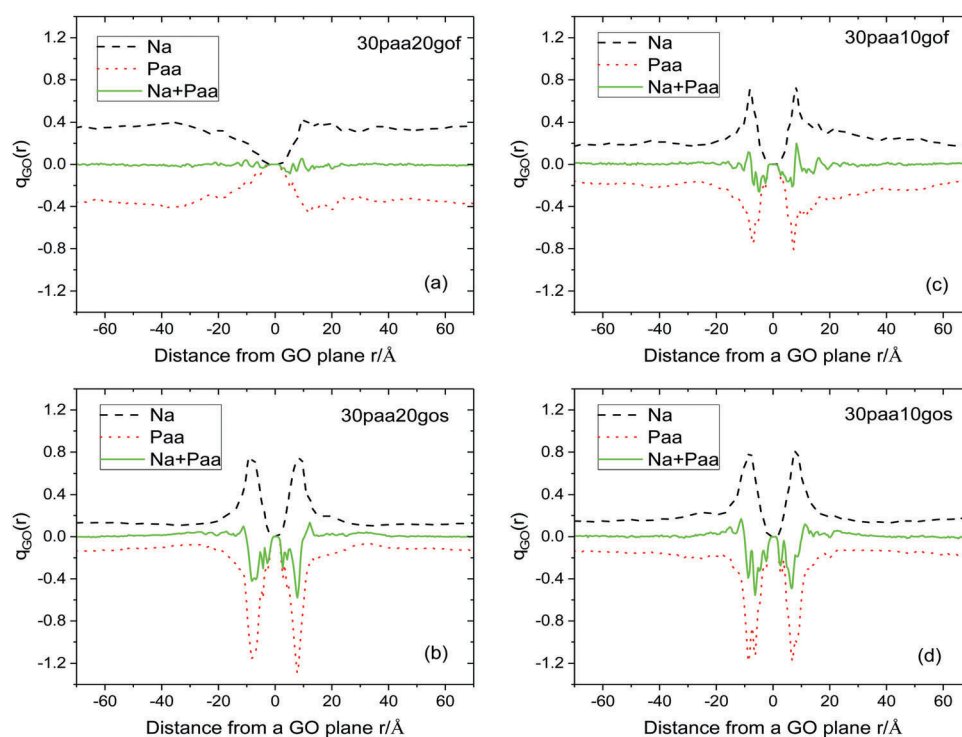

Fig. 5 Charge distributions arising from the PAA chains (dotted lines) and the counterions (dashed lines), in a direction normal to a GO flake. The 0 value denotes the location of the GO plane.

direction perpendicular to a GO platelet as a function of distance from its plane. The GO plane was defined by its center of mass and the two directions of the eigenvectors of the inertia tensor (eqn (1)) that approximately lie parallel to the GO sheet.

In the case of systems with fully charged chains (Fig. 5a and c), it appears that the concentration of counterions close to the interface is such that it practically neutralizes the charge arising from the PAA monomers. There exist small fluctuations of the total charge in the 30paa10gof system, but still these fluctuations involve negative as well as positive charge excesses. Apparently, this is not the case for systems involving semi-charged chains. In these systems a net negative charge remains

close to the GO surface due to an increased localization of polymer charges at the interface. This surface overcharging effect[65] may trigger an increased electrical response of these hydrogels since on one hand there is a higher percentage of non-condensed counterions (Fig. 4b) while on the other hand the GO surface bears an effective negative charge. Rationalization of this behavior can be envisaged through a sensitive balance between enthalpic and entropic interactions which affect the overall free energy of the system. Localization of polymer charges close to the neutral GO surface imparts a reduction of the chain configurational entropy, which, however, could be compensated by the gain in entropy due to the higher percentage of uncondensed

counterions[66] and the favorable PAA/GO enthalpic interfacial interactions as will be discussed in the section to follow.

3.2. Polymer adsorption onto GO surface/interfacial interactions

To elaborate more on the affinity between PAA and GO, we calculated the potential of mean force, $w(r)$, between the two moieties, based on the pair correlation function $g(r)$ arising from their centers of mass, according to

$$g(r) = e^{-\frac{w(r)}{KT}} \qquad (3)$$

where K is Boltzmann's constant and T the temperature. Fig. 6 presents $w(r)$ in KT units for the composite models. Visual inspection of the calculated spectra shows the marked differentiation between the models bearing PAA chains at the semi- and those at the fully charged state. In both samples based on semi-charged polymers the pair potential is mostly attractive up to about 40 Å separation, whereas in those based on fully charged chains, it is mostly repulsive or neutral. This implies more favorable interactions between the polymer and GO when the degree of Coulombic screening due to counterion condensation on PAA chains is lower. The differences observed between the 10 GO and the 20 GO systems might be related to the better statistics in the 20 GO systems since the number of PAA/GO pairs considered, scales with the number of the GO flakes. Other than that, at these low GO loadings, the affinity between a PAA chain and a GO flake is not expected to depend on GO concentration.

To check the relative tendency of polymer adsorption on the GO surface at a more local scale, we estimated the polymer density profiles along a direction normal to the GO surface at varying distances from a GO plane, as portrayed in Fig. 7. Evidently, the local density close to the GO surface is much more enhanced in the models containing the semi-charged PAA chains. In systems
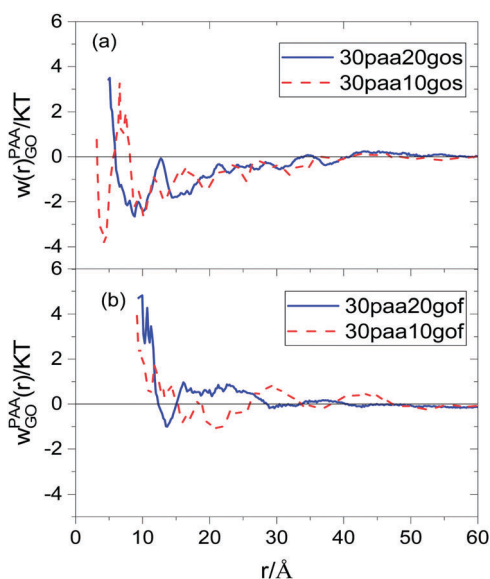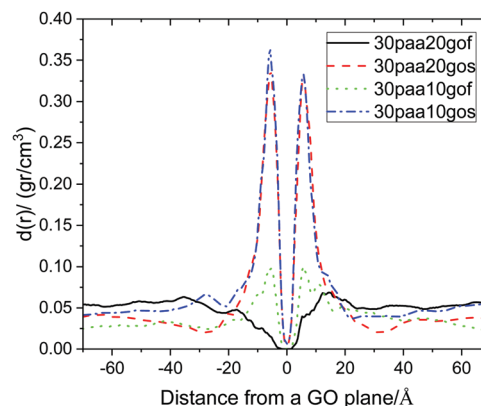

Fig. 7 Polymer density profiles in a direction normal to the GO surface as a function of distance from the GO plane.

bearing the fully charged polymer, the density peaks close to GO are either diminished (30paa10gof) or even suppressed (30paa20gof).

In a previous work it was found that a key interaction which promotes the dispersion of GO flakes in a PAA matrix is hydrogen bonding, involving the polar oxygen groups of the two moieties.[67] These hydrogen-bonding pairs involve the hydroxyl hydrogens (HO) of PAA and the epoxide oxygens (OS) of GO, the hydroxyl hydrogens of GO, and the carboxyl oxygens (O) of PAA, and the hydroxyl hydrogens and hydroxyl oxygens (OH) of both moieties.

To monitor the degree of hydrogen bonding between GO and PAA in the examined models, we adopted geometric criteria based on the hydrogen–acceptor (H–A) distance and the angle formed by the donor–hydrogen–acceptor (D–H–A) atoms. For this purpose we calculated the H–A pair distribution function of pairs belonging to D–H–A angles higher than 120 degrees[68] and counted as hydrogen-bonded those whose separation was smaller than the first minimum of the distribution function.

Examples of such pair distribution functions used for the identification of hydrogen-bonded pairs are shown in Fig. S3 in the ESI.† The resulting hydrogen-bond populations appear in Fig. 8. In the fully charged systems, since no hydroxyl hydrogens are available, hydrogen bonding with GO can only be realized between the hydroxyl hydrogens of GO and the oxygens in the COO^- group of PAA. Therefore, the degree of GO–PAA hydrogen bonding is significantly higher in models based on the semi-charged PAA chains. In these systems the HO–OH pairs are more abundant (since hydroxyl hydrogens and hydroxyl oxygens are available in both moieties for hydrogen bonding), followed by the HO–O pairs. The degree of hydrogen bonding appears to scale with the number of the GO flakes (so that after normalization with the number of GO sheets between the 10 GO and 20 GO systems, the picture would be similar). In other words, although the nature of hydrogen bonding between the two moieties does not change when increasing the GO loading, the presence of a higher number of GO flakes contributes toward an overall higher degree of physical association between the polymer and GO. This picture verifies conjectures made after

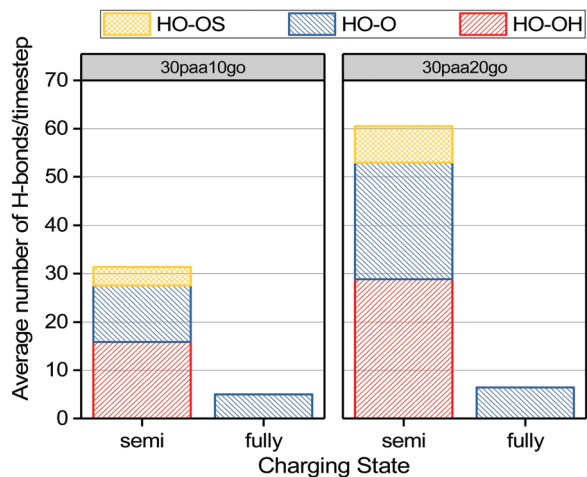Fig. 6 Potential of mean force between PAA chains and GO flakes.

Fig. 8 Average number of hydrogen bonds of GO–PAA hydrogen-bonding-capable pairs in the composite systems of the two different polymer charging states.
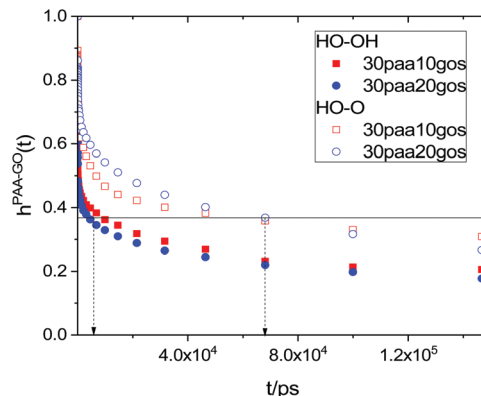

Fig. 9 Hydrogen bond correlation functions for the HO (GO, PAA)–OH (GO, PAA) and the O (PAA)–HO (GO) pairs in the systems based on the semi-charged polymers. The horizontal line corresponds to the $1/e$ value. The dotted vertical arrows denote the timescale at which the correlation functions have approximately attained the $1/e$ level.

experimental observations regarding the importance of hydrogen bonding in the formation of GO-based hydrogels in the presence of hydrogen-bonding-capable polymers, where GO acted as a physical gelator agent,[35] and provides insight to findings regarding dependence of the gelation process on the polymer/GO ratio.[18]

Apart from the absolute number of the PAA/GO hydrogens bonds, their relative lifetime is of interest, given the role it can play regarding the phase behavior[69] and the overall mechanical response[70] of polymer-based physical hydrogels. To extract this information we evaluated a hydrogen bond correlation function[71]

$$h(t) = \frac{\langle g(t)g(0)\rangle}{\langle g^2 \rangle} \quad (4)$$

where $g(t) = 1$ if the examined pair formed a hydrogen bond at time t provided that it was hydrogen bonded at time $t = 0$ as well, and 0 otherwise. Angle brackets denote ensemble average over all pairs and time origins. According to this definition, any possible dissociation of the hydrogen bond in the intermediate time interval between $t = 0$ and t is disregarded. Therefore, it is sensitive not to the first-breaking event but rather to the long time behavior which relates to the probability of the atoms that initially formed a hydrogen bond to remain at close proximity, and in an appropriate orientation, in order to form a hydrogen bond again. Such correlation functions are presented for the more abundant HO–OH and O–HO hydrogen bonded pairs in systems based on the semi-charged PAA chains, in Fig. 9.

Practically, there is no difference regarding the dynamic behavior of the hydrogen bonded pairs when comparing the 10 GO and 20 GO models. There is, however, a marked differentiation concerning the decay rate of the correlation functions when comparing the two different hydrogen bonded pairs. Those describing the HO (GO)–O (PAA) pairs decay with a much lower rate. To get an estimation of the difference on the characteristic decay timescales describing the two hydrogen-bonded pairs, we examined the time it takes for the correlation functions to drop to

the $1/e$ of their initial value, as shown schematically by the arrows in Fig. 9. This procedure rendered values of 5850 ps and 68 020 ps for the HO–OH and the O–HO pairs, respectively. Therefore, the lifetime of the latter (which involves the negatively charged PAA oxygen atom) is about one order of magnitude longer compared to that of the HO–OH hydrogen bonds and thus is expected to play a key part in the physical association of the two components. Although the number of the charged oxygen atoms per chain are twice as many in the fully charged models, their charge is more effectively screened by the counterions and the mean potential between PAA chains and GO is less attractive as discussed earlier, so the chance of hydrogen bonding between the hydroxyl hydrogens of GO and the charged oxygens of PAA remains very low in these systems.

3.3. Polymer dynamics

Knowledge of dynamics at different length scales in polymer hydrogels can be particularly useful in applications such as in controlled drug delivery[72] and in sensing,[73] since pertinent phenomena related to the targeted efficiency are realized at timescales relevant to a polymer's local and global motion. We monitored the PAA response at dimensions corresponding to the entire chain and to the length scale of a bond for the dynamic characterization of our systems, examining the average behavior (which most of the relevant experimental techniques are sensitive to), but also looking at the dynamic behavior close to the polymer/filler interface.

3.3.1 Polymer dynamics at the length scale of the polymer chain. The dynamic probes we employed are aimed at characterizing different aspects of chain dynamics, such as size fluctuations and the overall rotational and translational motion. Size fluctuations were examined by calculating the time correlation of the fluctuations of the squared radius of gyration (R_g) according to expression (5).

$$C_{R_g}(t) = \frac{\langle R_g^2(0) R_g^2(t)\rangle - \langle R_g^2 \rangle^2}{\langle R_g^4 \rangle - \langle R_g^2 \rangle^2} \quad (5)$$

This function is sensitive to the "breathing" mode of a polymer chain. The overall chain rotational motion was probed by monitoring the second order correlation function of unit vectors $\hat{k}(t)$ connecting the center of mass of a polymer chain with its atoms, as formulated in eqn (6).

$$C_2(t) = \frac{1}{2}\left\langle 3\left[\hat{k}(t)\cdot\hat{k}(0)\right]^2 - 1\right\rangle \tag{6}$$

Chain reorientational motion can be experimentally probed *via* dielectric relaxation spectroscopy measurements.[74] Polymer translational motion was followed by evaluating the intermediate incoherent dynamic structure factor arising from the center of mass of the PAA chains given by eqn (7).

$$S^{cm}(q,t) = \frac{1}{N}\sum_n \left\langle \exp[i\mathbf{q}\cdot(\mathbf{r}_n(t) - \mathbf{r}_n(0))]\right\rangle \tag{7}$$

In eqn (7), $\mathbf{q}$ represents the scattering vector whose magnitude is equal to q, and $\mathbf{r}_n(t)$ the position vector of the n-th scatterer (each center of mass of a chain represents a scatterer) at time t, and N is the number of polymer chains (here 30). The intermediate dynamic structure factor can be measured *via* neutron scattering experiments.[75] In order to focus on structural relaxation arising from translational motion of the centers of mass, we evaluated $S^{cm}(q,t)$ at a q magnitude corresponding to the first peak of the pertinent coherent static structure factor, denoted as $q*$ henceforth (see details in ESI,† eqn (S1) and Fig. S4). Correlation functions described by eqn (5), (6) and (7) are depicted in Fig. 10. A cursory glance on the dynamic spectra presented in this figure implies that correlation functions describing chain size fluctuations (Fig. 10a) have decayed to a lower extent compared to the two other kinds of motion.

This indicates rather persistent chain conformations at timescales at least of the order of several hundred ns. Judging from their relative degree of decorrelation, the faster size changes are realized in the model of semi-charged PAA chains in water without the presence of GO, while the slowest take place in the PAA/water system with the fully charged chains. This might be related to a more persistent nature of the larger aggregates formed in PAA/water systems when the chains are fully charged (see the relevant snapshots in Fig. 2). The observation that in the presence of GO, the semi-charged chain models show slower size dynamics than in the corresponding PAA/water system could be related to the fact that their association with GO renders them less deformable resulting in longer timescales for size changes. On the other hand, the fact that when GO is present, dynamics of fully charged chains becomes faster than in the corresponding PAA/water systems can be rationalized if we take into account that in this case GO intervenes against the formation of large polymer clusters (see snapshots in Fig. 2); the resulting smaller PAA aggregates are then more likely to be deformed at shorter timescales compared to those required for larger ones.

In the presence of GO, models based on the semi-charged polymer exhibit faster dynamics than those in which PAA is fully charged. This finding could be accounted for if the polymer adsorption/desorption process in semi-charged systems is
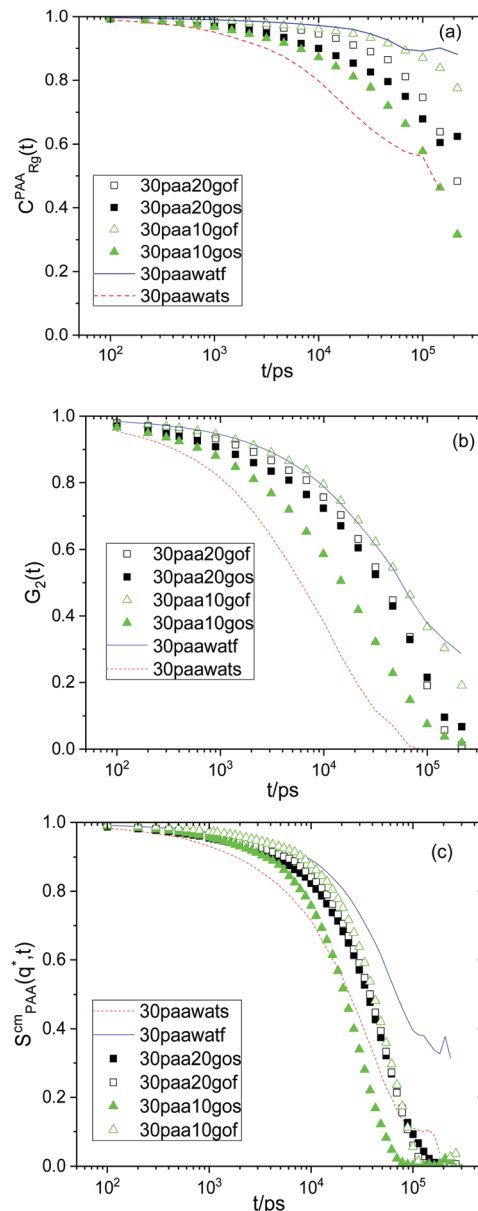

Fig. 10 Time correlation functions describing size fluctuations (a), rotational (b) and translational motion (c), of PAA chains.

realized at a shorter timescale, compared to that required for the size deformation of PAA chains belonging to the aggregates formed in the systems with the fully charged polymer.

The same general trends also characterize the chain rotational motion, alluding to a coupling with chain size fluctuations. The relevant timescales, though, appear faster than the timescale of the latter (note the considerably higher degree of decorrelation of spectra in Fig. 10b, compared to that of spectra in Fig. 10a). For translational motion of the chain centers of mass, the GO-based models exhibit rather similar decorrelation rates between them. To better visualize the differences in relaxation times between chain rotational and translational motion, we calculated a characteristic time $\tau_{1/e}$, at which the respective correlation times drop to $1/e$ of their initial value, as shown in Fig. 11.
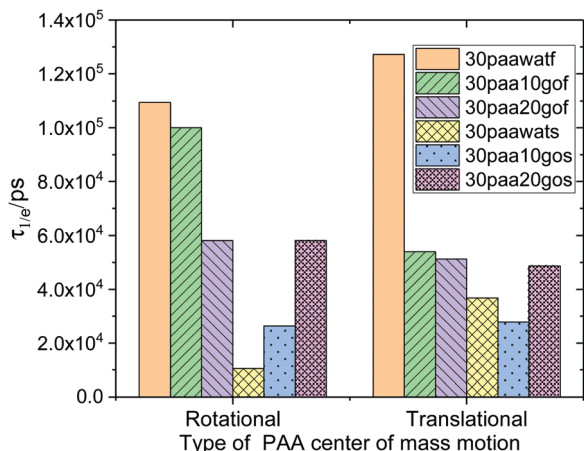
Fig. 11 Chain translational and rotational relaxation times of the simulated models.

A general pattern emerging from Fig. 11 is that the two motional mechanisms assume relaxation times of the same order of magnitude (with the higher deviation observed in the 30paa10gof system). This notion suggests a coupling between these two types of chain relaxation, as well. The differences become smaller in the systems with a higher GO loading, which can be taken as an indication of a stronger coupling, consistent with the larger number of PAA/GO contacts (see Fig. 8). The somewhat higher timescales characterizing the fully charged PAA/water model can be attributed to the larger polymer aggregates formed in this system, as argued earlier. Examination of chain dynamics close to the GO surface (see ESI,† Fig. S5) showed that in the models based on semi-charged chains, diffusive motion in the direction normal to the GO plane tends to be slower than the average.

In the case of models with fully charged chains, where practically no polymer adsorption onto GO occurs, the chain translational motion close to the interface appears (within the simulation's accuracy) to be almost indistinguishable from the overall average.

3.3.2 Polymer dynamics at the length scale of a bond.
Dynamics at the bond length scale was examined by evaluating rotational relaxation functions (referred to as $b_2(t)$) adopting an

expression analogous to eqn (6), but in this case $\hat{k}(t)$ represented a unit vector along the examined bond. The $b_2(t)$ function probes the re-orientational motion of a bond. Its Fourier transform is related to measurements of Neutron Magnetic Resonance (NMR) experiments.[76] To check both, bond dynamics along the backbone and at the carboxyl side group (see Fig. 1), we monitored the backbone carbon–carbon bond (C–C) and the carbon–oxygen bond (C–O) involving the negatively charged oxygen atom. The pertinent spectra are portrayed in Fig. 12. For both kinds of bonds, spectra describing systems based on the fully charged polymer chains, decorrelate with a lower rate (i.e., the motion is slower) showing only a moderate dependence on GO loading. In contrast, those corresponding to models based on semi-charged PAA chains exhibit a stronger dependence of the respective decorrelation rates on the percentage of GO.

Applying a procedure similar to that followed in Section 3.3.1, we estimated for each system the time it takes for the drop of the correlation functions to $1/e$. The corresponding times are illustrated in Fig. 13.

Apart from visualizing the aforementioned observations, it also becomes evident from Fig. 13 that the re-orientational motion of the side-group C–O bonds is realized on average at a shorter timescale compared to that of the backbone C–C bond. Although, in general, side group local polymer dynamics (usually associated with secondary relaxations) are expected to be faster compared to that of backbone-related motions,[77] in systems like those we examine here they are not straightforward to predict, since the relevant timescales might depend on the strength of the polymer/GO interactions and thus on the GO content (as is shown for our models as well). Another trend emerging from Fig. 13 is that upon increasing the GO content, bond dynamics related to the fully charged PAA chains become faster, while those associated with models based on semi-charged chains become slower.

To rationalize behavior observed in the fully charged models, we must take into account that in large molecular aggregates or in bulky polymer molecules,[78] complete relaxation of bond re-orientational motion requires overall rotation of the molecular aggregate or the bulky polymer. As discussed in Section 3.3.1, increasing the GO content may result in smaller chain aggregates and thus faster overall rotational motion (see Fig. 11),
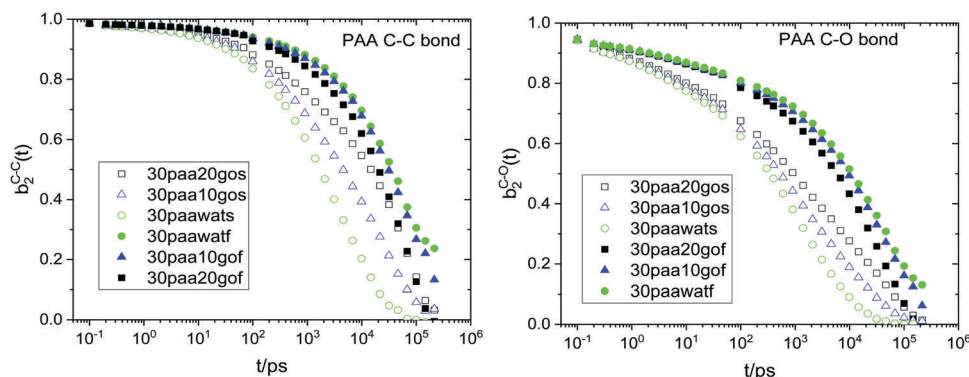

Fig. 12 Comparison of the bond re-orientational functions for the backbone C−C bond and the side-group C−O bond.
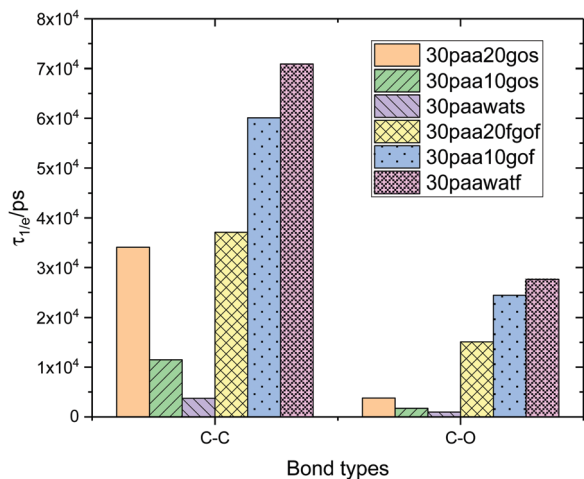
Fig. 13 Characteristic relaxation times $\tau_{1/e}$ describing the bond reorientational functions shown in Fig. 12.

thus leading to faster bond reorientation as well. On the other hand, in models with semi-charged polymer chains, increase of the GO content leads to slowing down of the overall chain reorientation (see Fig. 11), while, on top of that, a growing percentage of bonds physically adsorb onto GO flakes (Fig. 8).

The dynamic response of backbone (C–C) or side-group (C–O) PAA bonds located at the 1st adsorption layer (see ESI,† Fig. S6), was found to be slower and with modified spectral characteristics compared to the average behavior, thus demonstrating a different local environment experienced by bonds close to the polymer/filler interface. It was also found that bond re-orientational motion close to the GO surface was not affected by the GO content, at the examined GO loading; this, however, might not be the case in more concentrated systems where the number of polymer/GO contacts per GO sheet could increase significantly, which, when combined with an increase in the viscosity and a possible change in the polymer/water interaction,[79] could lead to a concentration-dependent degree of slowing down near the interface.

3.4 Dynamics of counterions

The dynamics of counterions, apart from its direct association with the system's conductivity, is also known to play a significant

part in nanoscale processes related to effective molecular interactions in polyelectrolyte systems,[80] particularly when it comes to the counterion-mediated attraction between like-charged macromolecules and overcharging phenomena,[81–84] such as those observed in the systems studied here (see Fig. 2 and 5). When sufficiently strong electrostatic interactions are present, it has been found[85–87] that distinct phases of counterions can be formed corresponding to condensed and uncondensed populations. This picture is relevant to our case given the different degrees of counterion condensation observed in the models based on semi- and fully charged PAA chains (see Fig. 4). A sensitive probe for the characterization of particles' motion in terms of their relative mobility is the Van Hove correlation function.[88] Its self-part is given by eqn (8)

$$G_{s}(r,t) = \frac{1}{N}\left\langle \sum_{i} \delta[r - |\boldsymbol{r}_i(t) - \boldsymbol{r}_i(0)|] \right\rangle \quad (8)$$

where N represents the total number of particles, δ is the Dirac's function, $\boldsymbol{r}_i(t)$ is the position vector of the ith particle at time t and r symbolizes the distance between the positions of the ith particle at times t and 0. This function is proportional to the probability that a particle is at position $\boldsymbol{r}$ at time t given that the same particle was at the origin ($\boldsymbol{r}$ = 0) at time t = 0. It essentially probes self-motion as a function of time and is related *via* its Fourier transform to the incoherent dynamic structure factor that was discussed earlier. In case the population of the particles probed (here the counterions) perform homogeneous motion, then the distance they travel at different time periods is normally distributed so that $G_{s}(r,t)$ takes a Gaussian form. In this case the peak location indicates the most probable distance travelled by the particles within the considered time interval t. If the particles under examination undergo diffusion in an inhomogeneous environment (*e.g.*, their motion is inhibited), then deviations from Gaussian behavior may grow sufficiently strong to the point where particle populations with distinctly different mobilities are formed. Fig. 14 presents the self Van Hove functions of the counterions in the examined systems at different time intervals.

The shape of the $G_{s}(r,t)$ curves of all the examined models implies the existence of two populations of counterions with distinct mobilities. The maximum corresponding to the first
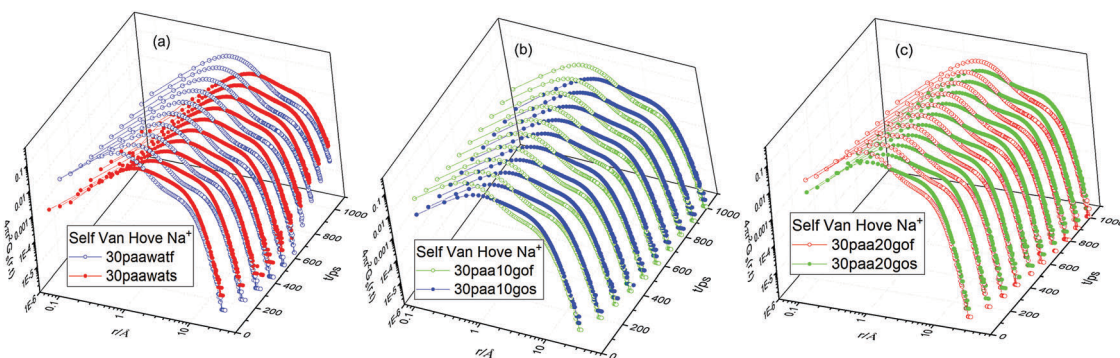

Fig. 14 Comparison of the self van Hove functions (multiplied by $4\pi r^2$) describing the counterions' motion in systems based on the semi- (filled symbols) and the fully charged (open symbols) polymer chains. (a) 30paawat systems, (b) 30paa10go systems, and (c) 30paa20go systems.

counterion population is located at short distances indicating a territorially bound motion, while the second population appears as a shoulder in the spectra at longer distances. The difference between the distances travelled by these two populations increases as time lapses. This picture alludes to the identification of the maximum at shorter distances with the population corresponding to the counterions condensed (*i.e.*, rather tightly bound) on the oppositely charged PAA chains, while that appearing as a shoulder at longer distances, to the uncondensed counterions. A common characteristic shared by all pairs of systems corresponding to the same GO loading is that the intensity of the maximum representing the condensed counterions is higher (at all the examined timescales) when the PAA chains are fully charged. In addition, in the latter systems the separation in the distance travelled between the two populations appears to be larger, as is the difference in the relative height between the peaks representing the two populations. These features are consistent with the picture described in Section 3.2 regarding the degree of counterion condensation in the semi- and in the fully charged PAA based models.

To obtain a more detailed view on the effects of the charging state of PAA chains and of the GO percentage on the dynamics of counterions, we have compared relevant $G_s(r,t)$ spectra at a constant timescale in Fig. 15 (the results presented below do not depend on the timescale selected, see Fig. S7 in the ESI†). Focusing on the behavior of the systems based on the fully charged chains, it appears that an increase in GO loading results in a shift of the curves at longer distances, that is, increases the average mobility of the counterions. This effect is stronger in the
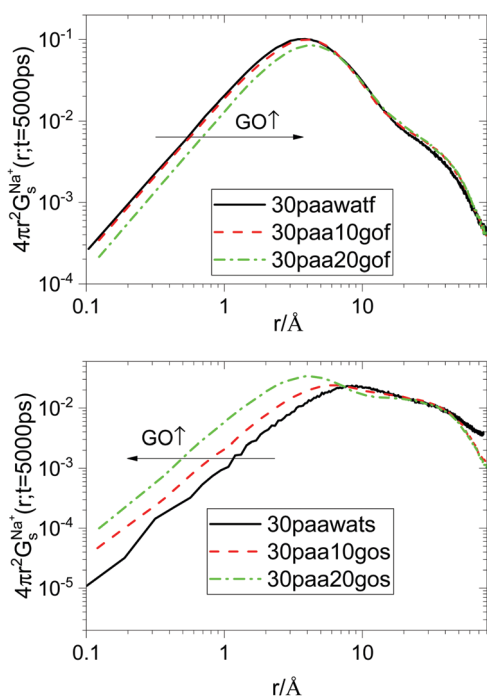
system with the higher GO content. The opposite trend characterizes behavior in the systems based on semi-charged chains. In this case, the mobility of the counterions decreases at an even higher degree upon increase of the GO loading, compared to the degree of the speed-up observed in systems with fully charged chains. This behavior of counterion mobility can be correlated to that noted in polymer dynamics at global and local length scales as discussed in Sections 3.3.1 and 3.3.2. In other words, it appears that counterion mobility (particularly that of the more localized population) is coupled with polymer motion at the nanoscale, in line with relevant experimental findings in flexible polyelectrolyte solutions.[89]

A way to obtain a measure of residence time of the counterions in the condensed phase is to calculate a correlation function analogous to that of eqn (4), examining the dynamic formation/breaking of pairs between counterions and the negatively charged oxygens of PAA. In this case, $g(t)$ of eqn (4) takes a value of 1 if the examined atoms form a pair at time t provided that they also formed a pair at time $t = 0$, and 0. The criterion for pair formation was based on the respective pair correlations functions as discussed in Section 3.2 (no directionality was taken into account in this case). The so-calculated residence correlation functions are plotted in Fig. 16.

Evidently, the residence correlation functions are grouped together depending on the charging state of the polymer chains. Those corresponding to systems with the fully charged polymer decorrelate at much lower rates, indicating a much stronger binding between PAA and counterions. Estimation of characteristic times based on the drop of the correlation functions to $1/e$, yields residence times between 4.0 and 5.5 ns for the semi-charged PAA systems and between 40 and 100 ns approximately for those with the fully charged chains.

The dependence of the residence time of counterions in the bound layer on GO loading, is much stronger in systems involving fully charged chains. In these systems residence times decrease as GO loading grows, in line with the increasing mobility probed by the pertinent Van Hove functions (Fig. 15, upper panel) and with the decreasing intensity of the charge distributions around a PAA chain (see Fig. S2 in the ESI†), which imply diminishing strengths of the formed counterion/polymer-charge dipoles.[90] Such changes

Fig. 15 Comparison of self van Hove spectra of counterions at t = 5000 ps for systems based on fully (upper) and semi-charged (lower) PAA chains. The direction of the arrow denotes the direction of increase of the GO loading.
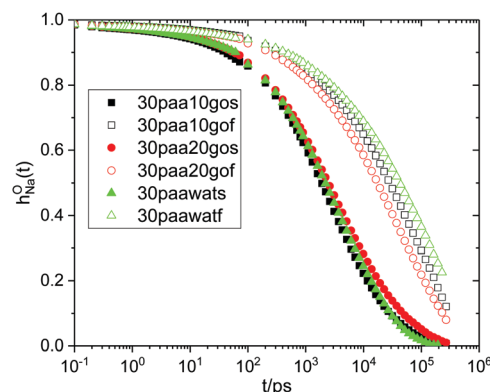

Fig. 16 Residence correlation functions (see text) of Na$^+$–O$^-$ pairs.

in the local dielectric environment experienced by the counterions at constant polymer charging state but varying GO content, essentially reveal another aspect regarding the role of GO in counterion mobility and thus in the counterion-related electric behavior of such systems.

4. Conclusions

In this study we examined for the first time by means of molecular dynamics simulations at fully atomistic detail, composite hydrogels based on poly(acrylic acid), nanoflakes of graphene oxide and explicit neutralizing counterions. Two different charging states of the polymer (that could be experimentally realized by altering pH) were considered (*i.e.*, 100% and 50% of monomer charging) and also two different GO concentrations, approximately 2% and 4% in weight. We monitored static and dynamic properties of the polymeric component and the counterions, relevant to aspects of the mechanical and electrical response of such materials.

It was found that the charging state of the polyelectrolyte affected drastically the internal structure of the hydrogels. In the systems based on semi-charged chains, an interconnected GO/PAA morphology was observed, where polymer association with GO was promoted through hydrogen bonding. In these systems, the physical adsorption of polymer chains onto the GO surface resulted in an effective overcharging of the GO flakes. In contrast, in systems based on the fully charged PAA chains, the more effective screening of the electrostatic interactions led to formation of polymer aggregates, the characteristics of which depended on GO loading.

The distinct morphological features characterizing the systems with a different charging state of the PAA chains strongly affected polymer dynamics in global and local length scales and the motional mechanisms of the counterions. Increase of the GO loading in the systems with the semi-charged chains resulted in an overall slowing down of polymer dynamics, while an opposite trend was noticed in the systems with fully charged chains.

Two distinct counterion populations could be distinguished in terms of their mobilities, arising from the ions condensed on the polymer chains and from their uncondensed counterparts. Counterion dynamics was found to be coupled with the polymer motion. This behavior implies that GO loading, apart from the role that it is anticipated to play in the mechanical response of these systems, is also expected to play a significant part in their ionic conductivity.

Several of the conclusions drawn above for the PAA/GO hydrogels could also apply to a broader range of polyelectrolyte/GO systems bearing similar features to those examined here, such as a pH-dependent degree of charging of the polymer chains in an aqueous environment, presence of monovalent counterions, existence of hydrogen-bonding-capable groups, low GO loadings and polymer concentrations well below the overlapping limit. We therefore believe that this work could form the basis upon which the behavior of similar or even more complex GO-based composite hydrogels could be analysed and interpreted following theoretical or experimental approaches.

Conflicts of interest

The authors declare no competing financial interests.

Acknowledgements

References

1 L. Yu and J. Ding, *Chem. Soc. Rev.*, 2008, **37**, 1473.
2 B. V. Slaughter, S. S. Khurshid, O. Z. Fisher, A. Khademhosseini and N. A. Peppas, *Adv. Mater.*, 2009, **21**, 3307–3329.
3 J. C. Tiller, *Angew. Chem., Int. Ed.*, 2003, **42**, 3072–3075.
4 Y.-Y. Chen, H.-C. Wu, J.-S. Sun, G.-C. Dong and T.-W. Wang, *Langmuir*, 2013, **29**, 3721–3729.
5 Y. Li, G. Huang, X. Zhang, B. Li, Y. Chen, T. Lu, T. J. Lu and F. Xu, *Adv. Funct. Mater.*, 2012, **23**, 660–672.
6 Y. Zheng and A. Wang, *J. Hazard. Mater.*, 2009, **171**, 671–677.
7 X.-J. Ju, S.-B. Zhang, M.-Y. Zhou, R. Xie, L. Yang and L.-Y. Chu, *J. Hazard. Mater.*, 2009, **167**, 114–118.
8 A. Guiseppi-Elie, *Biomaterials*, 2010, **31**, 2701–2716.
9 L. A. Estroff and A. D. Hamilton, *Chem. Rev.*, 2004, **104**, 1201–1218.
10 P. Calvert, *Adv. Mater.*, 2009, **21**, 743–756.
11 Y. Tang, C. L. Heaysman, S. Willis and A. L. Lewis, *Expert Opin. Drug Delivery*, 2011, **8**, 1141–1159.
12 S. J. de Jong, B. van Eerdenbrugh, C. F. van Nostrum, J. J. Kettenes-van den Bosch and W. E. Hennink, *J. Controlled Release*, 2001, **71**, 261.
13 F. Liu, S. Chung, G. Oh and T. S. Seo, *ACS Appl. Mater. Interfaces*, 2012, **4**, 922–927.
14 J. Kopeček and J. Yang, *Angew. Chem., Int. Ed.*, 2012, **51**, 7396–7417.
15 Y. Xu, K. Sheng, C. Li and G. Shi, *ACS Nano*, 2010, **4**, 4324–4330.
16 M. Chau, K. J. De France, B. Kopera, V. R. Machado, S. Rosenfeldt, L. Reyes, K. J. W. Chan, S. Förster, E. D. Cranston, T. Hoare and E. Kumacheva, *Chem. Mater.*, 2016, **28**, 3406–3415.
17 K. Haraguchi, *Curr. Opin. Solid State Mater. Sci.*, 2007, **11**, 47–54.
18 H. Bai, C. Li, X. Wang and G. Shi, *Chem. Commun.*, 2010, **46**, 2376–2378.
19 Y. Huang, M. Zeng, J. Ren, J. Wang, L. Fan and Q. Xu, *Colloids Surf., A*, 2012, **401**, 97–106.
20 N. Zhang, R. Li, L. Zhang, H. Chen, W. Wang, Y. Liu, T. Wu, X. Wang, W. Wang, Y. Li, Y. Zhao and J. Gao, *Soft Matter*, 2011, 7, 7231.

21 W. Cai, R. D. Piner, F. J. Stadermann, S. Park, M. A. Shaibat, Y. Ishii, D. Yang, A. Velamakanni, S. J. An, M. Stoller, J. An, D. Chen and R. S. Ruoff, *Science*, 2008, **321**, 1815–1817.

22 V. Sridhar and I.-K. Oh, *J. Colloid Interface Sci.*, 2010, **348**, 384–387.

23 Y. Piao and B. Chen, *J. Polym. Sci., Part B: Polym. Phys.*, 2015, **53**, 356–367.

24 J. J. Liang, Y. Huang, L. Zhang, Y. Wang, Y. F. Ma, T. Y. Guo and Y. S. Chen, *Adv. Funct. Mater.*, 2009, **19**, 2297–2302.

25 J. Fan, Z. Shi, M. Lian, H. Li and J. Yin, *J. Mater. Chem. A*, 2013, **1**, 7433.

26 S. Sun and P. Wu, *J. Mater. Chem.*, 2011, **21**, 4095.

27 A. Servant, V. Leon, D. Jasim, L. Methven, P. Limousin, E. V. Fernandez-Pacheco, M. Prato and K. Kostarelos, *Adv. Healthcare Mater.*, 2014, **3**, 1334–1343.

28 H. Guo, T. Jiao, Q. Zhang, W. Guo, Q. Peng and X. Yan, *Nanoscale Res. Lett.*, 2015, **10**, 272.

29 M. Hu, S. Zheng and B. Mi, *Environ. Sci. Technol.*, 2016, **50**, 685–693.

30 F. Shao, L. Dong, H. Dong, Q. Zhang, M. Zhao, L. Yu, B. Pang and Y. Chen, *J. Membr. Sci.*, 2017, **525**, 9–17.

31 C. Cheng, Z. Liu, X. Li, B. Su, T. Zhou and C. Zhao, *RSC Adv.*, 2014, **4**, 42346–42357.

32 H. Bai, K. Sheng, P. Zhang, C. Li and G. Shi, *J. Mater. Chem.*, 2011, **21**, 18653–18658.

33 B. Berke, O. Czakkel, L. Porcar, E. Geissler and K. Laszlo, *Soft Matter*, 2016, **12**, 7166–7173.

34 J. Kamcev, M. Galizia, F. M. Benedetti, E.-S. Jang, D. R. Paul, B. D. Freeman and G. S. Manning, *Phys. Chem. Chem. Phys.*, 2016, **18**, 6021–6031.

35 H. Bai, C. Li, X. Wang and G. Shi, *J. Phys. Chem. C*, 2011, **115**, 5545–5551.

36 J. Shen, B. Yan, T. Li, Y. Long, N. Li and M. Ye, *Soft Matter*, 2012, **8**, 1831–1836.

37 Z. Tai, J. Yang, Y. Qi, X. Yan and Q. Xue, *RSC Adv.*, 2013, **3**, 12751–12757.

38 S. Lee, H. Lee, J. Sim and D. Sohn, *Macromol. Res.*, 2014, **22**, 165–172.

39 M. Zhong, Y.-T. Liu and X.-M. Xie, *J. Mater. Chem. B*, 2015, **3**, 4001–4008.

40 H. Xiao, J. P. Pender, M. A. Meece-Rayle, J. P. de Souza, K. C. Klavetter, H. Ha, J. Lin, A. Heller, C. J. Ellison and C. B. Mullins, *ACS Appl. Mater. Interfaces*, 2017, **9**, 22641–22651.

41 J. Choi and M. F. Rubner, *Macromolecules*, 2005, **38**, 116–124.

42 Q. Cao and M. Bachmann, *Chem. Phys. Lett.*, 2013, **586**, 51–55.

43 D. Stauffer, N. Dragneva, W. B. Floriano, R. C. Mawhinney, G. Fanchini, S. French and O. Rubel, *J. Chem. Phys.*, 2014, **141**, 044705.

44 A. Bagri, C. Mattevi, M. Acik, Y. J. Chabal, M. Chhowalla and V. B. Shenoy, *Nat. Chem.*, 2010, **2**, 581–587.

45 W. D. Cornell, P. Cieplak, C. I. Bayly, I. R. Gould, K. M. Merz, D. M. Ferguson, D. C. Spellmeyer, T. Fox, J. W. Caldwell and P. A. Kollman, *J. Am. Chem. Soc.*, 1995, **117**, 5179–5197.

46 D. J. Sparks, M. E. Romero-Gonzalez, E. El-Taboni, C. L. Freeman, S. A. Hall, G. Kakonyi, L. Swanson, S. A. Banwart and J. H. Harding, *Phys. Chem. Chem. Phys.*, 2015, **17**, 27357–27365.

47 Z. Adamczyk, A. Bratek, B. Jachimska, T. Jasinski and P. Warszynski, *J. Phys. Chem. B*, 2006, **110**, 22426–22435.

48 J. Wang, R. M. Wolf, J. W. Caldwell, P. A. Kollman and D. A. Case, *J. Comput. Chem.*, 2004, **25**, 1157–1174.

49 J. Wang, W. Wang, P. A. Kollman and D. A. Case, *J. Mol. Graphics Modell.*, 2006, **25**, 247260.

50 W. L. Jorgensen, J. Chandrasekhar, J. D. Madura, R. W. Impey and M. Klein, *J. Chem. Phys.*, 1983, **79**, 926.

51 D. Li, M. B. Muller, S. Gilje, R. B. Kaner and G. G. Wallace, *Nat. Nanotechnol.*, 2008, **3**, 101–105.

52 G. Wang, J. Yang, J. Xinglong, B. Wang and J. HaoYao, *J. Phys. Chem. C*, 2008, **112**, 8192–8195.

53 H. Zhou, C. Cheng, H. Qin, L. Ma, C. He, S. Nie, X. Zhang, Q. Fu and C. Zhao, *Polym. Chem.*, 2014, **5**, 3563.

54 L. Martínez, R. Andrade, E. G. Birgin and J. M. Martínez, *J. Comput. Chem.*, 2009, **30**, 2157–2164.

55 S. E. Feller, Y. Zhang, R. W. Pastor and B. R. Brooks, *J. Chem. Phys.*, 1995, **103**, 4613–4621.

56 T. Darden, L. Perera, L. Li and L. Pedersen, *Structure*, 1999, **7**, R55–R60.

57 J. Phillips, R. Braun, W. Wang, J. Gumbart, E. Tajkhorshid, E. Villa, C. Chipot, R. Skeel, L. Kale and K. Schulten, *J. Comput. Chem.*, 2005, **26**, 1781–1782.

58 H. Tang, D. Liu, Y. Zhao, X. Yang, J. Lu and F. Cui, *J. Phys. Chem. C*, 2015, **119**, 26712–26718.

59 L. Gong, R. J. Young, I. A. Kinloch, I. Riaz, R. Jalil and K. S. Novoselov, *ACS Nano*, 2012, **6**, 2086–2095.

60 R. J. Young, I. A. Kinloch, L. Gong and K. S. Novoselov, *Compos. Sci. Technol.*, 2012, **72**, 1459–1476.

61 J. Rudnick and G. Gaspari, *J. Phys. A: Math. Gen.*, 1986, **19**, L191–L193.

62 T. Swift, L. Swanson, M. Geoghegan and S. Rimmer, *Soft Matter*, 2016, **12**, 2542–2549.

63 G. S. Manning, *J. Chem. Phys.*, 1969, **51**, 924–933.

64 *Conformation and Phase Diagrams of Flexible Polyelectrolytes*, ed. N. Volk, D. Vollmer, M. Schmidt, W. Oppermann and K. Huber, Springer Berlin Heidelberg, 2004.

65 A. V. Dobrynin and M. Rubinstein, *Prog. Polym. Sci.*, 2005, **30**, 1049–1118.

66 L. Sjostrom, T. Akesson and B. Jonsson, *J. Chem. Phys.*, 1993, **99**, 4739–4747.

67 K. Karatasos and G. Kritikos, *RSC Adv.*, 2016, **6**, 109267.

68 E. Chiessi, F. Cavalieri and G. Paradossi, *J. Phys. Chem. B*, 2007, **111**, 2820–2827.

69 S. Deshmukh, D. A. Mooney, T. McDermott, S. Kulkarni and J. M. Don MacElroy, *Soft Matter*, 2009, **5**, 1514–1521.

70 X. Hu, J. Zhou, W. F. M. Daniel, M. Vatankhah-Varnoosfaderani, A. V. Dobrynin and S. S. Sheiko, *Macromolecules*, 2017, **50**, 652–659.

71 D. C. Rapaport, *Mol. Phys.*, 1983, **50**, 1151–1162.

72 I. S. Raja and N. N. Fathima, *SpringerPlus*, 2014, **3**, 393.

73 H.-J. Schneider, K. Kato and R. M. Strongin, *Sensors*, 2007, **7**, 1578–1611.

74 *Broadband Dielectric Spectroscopy*, ed. F. Kremer and A. Schoenhals, Springer Berlin Heidelberg, 2003.

75 T. Pakula, in *Broadband Dielectric Spectroscopy*, Springer Berlin Heidelberg, 2003, pp. 597–623.

76 K. Karatasos, J. P. Ryckaert, R. Ricciardi and F. Lauprêtre, *Macromolecules*, 2002, **35**, 1451–1462.

77 R. Boyd and G. Smith, *Polymer Dynamics and Relaxation*, Cambridge University Press, 2007.

78 K. Karatasos, *Macromolecules*, 2014, **47**, 8833–8845.

79 H. Li, *Smart Hydrogel Modelling*, Springer Berlin Heidelberg, 2009.

80 T. S. Lo, B. Khusid and J. Koplik, *Phys. Rev. Lett.*, 2008, **100**, 128301.

81 Q. Xiangyun, A. Kurt, W. K. Lisa, S. L. Jessica, P. Hye Yoon and P. Lois, *Phys. Rev. Lett.*, 2007, **99**, 038104.

82 K. Karatasos, *Macromolecules*, 2008, **41**, 1025–1033.

83 T. E. Angelini, H. Liang, W. Wriggers and G. C. L. Wong, *Proc. Natl. Acad. Sci. U. S. A.*, 2003, **100**, 8634–8637.

84 S. V. Lyulin, K. Karatasos, A. Darinskii, S. Larin and A. V. Lyulin, *Soft Matter*, 2008, **4**, 453.

85 F. Bordi, C. Cametti and R. H. Colby, *J. Phys.: Condens. Matter*, 2004, **16**, R1423–R1463.

86 Y. Katsumoto, S. Omori, D. Yamamoto, A. Yasuda and K. Asami, *Phys. Rev. E: Stat., Nonlinear, Soft Matter Phys.*, 2007, **75**, 011911.

87 K. Karatasos and M. Krystallis, *J. Chem. Phys.*, 2009, **130**, 114903.

88 J.-P. Hansen and I. R. McDonald, *Theory of simple liquids*, Elsevier, Amsterdam, 3rd edn, 2006.

89 V. M. Prabhu, E. J. Amis, D. P. Bossev and N. Rosov, *J. Chem. Phys.*, 2004, **121**, 4424–4429.

90 M. Muthukumar, *J. Chem. Phys.*, 2004, **120**, 9343–9350.